Theor Chim Acta (1986) 70: 265-296

Theoretica Chimica Acta

Theoretical studies of hydrogen storage in binary Ti-Ni, Ti-Cu, and Ti-Fe alloys

Jozef Bicerano[1]*, John E. Keem[1], and H. Bernhard Schlegel[2]**

[1] Energy Conversion Devices, Inc., 1675 West Maple Road, Troy, MI 48084, USA
[2] Wayne State University, Department of Chemistry, Detroit, MI 48202, USA

(Received June 6/Accepted June 16, 1986)

Theoretical studies have been carried out to examine hydrogen storage in some binary transition metal alloys which include titanium as one of the alloying elements. Quantum mechanical calculations at the Extended Hückel level of approximation have been performed on numerous clusters of compositions $Ti_{18}Ni_{18}$, $Ti_{18}Ni_{18}H$, $Ti_{18}Ni_{18}H_{12}$, $Ti_{24}Ni_{12}$, $Ti_{24}Ni_{12}H$, $Ti_{24}Ni_{12}H_{12}$, $Ti_{16}Cu_{16}$, $Ti_{16}Cu_{16}H$, $Ti_{24}Cu_{12}$, $Ti_{16}Fe_{16}$, $Ti_{16}Fe_{16}H_9$, and $Ti_{16}Fe_{16}H_{32}$, to yield information on energetics, densities of states, charge distributions, and the effects of hydrogenation on these properties. In addition, *ab initio* calculations at the split valence level of approximation have been performed on several smaller clusters. The hydrogens have been shown to acquire a partially anionic character in all cases. Another conclusion is that the preference of H for certain types of sites (for example the tetrahedral Ti_4 sites in crystalline TiCu) is more likely to be related not to the intrinsically greater stability of a hydrogen atom located in such a site, but to more general topological and electronic considerations. Qualitative concepts related to the classification, spatial distribution, and sizes and shapes of "hole" sites which could become occupied by hydrogen atoms, have been shown to correlate with hydrogen storage capacity for crystalline materials. These qualitative concepts have been extended to amorphous materials and corroborate the observations that under optimized conditions amorphous alloys can be found with better reversible hydrogen storage properties than the crystalline or microcrystalline systems.

* *Current address*: Dow Chemical Company, Central Research, Materials Science and Engineered Products Laboratory, 1702 Building, Midland, MI 48674, USA
** Camille and Henry Dreyfus teacher-scholar

Distorted tetrahedral and octahedral holes have been examined in detail, and parameters (volume, area, "tetrahedrality", and "octahedrality") have been introduced to describe their sizes and shapes. An algorithmic surveying technique has been introduced, and shown to provide useful information about the limiting amounts of hydrogen uptake.

Key words: Hydrogen storage — Binary alloys — Transition metals — Titanium — Extended Hückel — *ab initio* — Sites — Volume — Area — Tetrahedrality — Surveying technique — Split valence — Metal hydrides

1. Introduction

We have carried out theoretical studies in order to elucidate a theory related to the relationships and interactions of d band elements that take place in three-dimensional space in amorphous and disordered materials, particularly in their interactions with hydrogen in both dissociation and storage [1]. The general field of hydrogen storage and interaction has become an interdisciplinary research undertaken in various areas of science and engineering, and primarily motivated by the potential of hydrogen as a chemical and nuclear energy carrier [2]. The alloys of hydrogen and metals (metal hydrides) have been investigated by a large number of theoretical [3] and experimental [4] techniques, the materials development effort being mainly directed toward the development of materials useful for the reversible storage of hydrogen and its isotopes. However, in spite of this vast body of research, much remains to be discovered in terms of their structural and electronic properties, the various mechanistic processes involved, the thermodynamic and kinetic factors of significance, and how all these complex and often competing factors can best be balanced to prepare materials especially suitable for specific technological applications.

We report here the results of our work on hydrogen storage in some binary transition metal alloys which include titanium as one of the alloying elements. Although we have mainly concentrated on Ti–Ni alloys, we have also considered some Ti–Cu and Ti–Fe systems. *Ab initio* unrestricted Hartree–Fock calculations have been performed on small clusters of compositions Ti_4, Ti_4H, Ti_2Ni_2, Ti_2Ni_2H, Ni_4 and Ni_4H. These calculations included all electrons and were carried out with minimal basis sets (with and without exponent optimization) and with split valence basis sets. Several different geometries were chosen to test the effects of the shape and the volume of the tetrahedral hole, as well as the composition of the cluster, on the binding of hydrogen.

Extended Hückel calculations [5] on the small metal clusters and their hydrides are in good qualitative agreement with the *ab initio* results. This serves to calibrate the Extended Hückel calculations on much larger clusters that are a better model of the bulk solid. Computations were performed on clusters of compositions $Ti_{18}Ni_{18}$, $Ti_{18}Ni_{18}H$, $Ti_{18}Ni_{18}H_{12}$, $Ti_{24}Ni_{12}$, $Ti_{24}Ni_{12}H$, $Ti_{24}Ni_{12}H_{12}$, $Ti_{16}Cu_{16}$, $Ti_{16}Cu_{16}H$, $Ti_{24}Cu_{12}$, $Ti_{16}Fe_{16}$, $Ti_{16}Fe_{16}H_9$, and $Ti_{16}Fe_{16}H_{32}$, to yield information on energetics, densities of states, charge distributions, and the effects of hydroge-

nation on these properties. Admittedly, the Extended Hückel method is approximate, but its simplicity and economy allow the performance of many calculations which would otherwise not be feasible. Valuable semi-quantitative information can be obtained if the results are appropriately calibrated and judiciously interpreted.

Qualitative concepts related to the classification into various types, spatial distribution, and sizes and shapes of "hole" sites which could become occupied by hydrogen atoms, have been shown to provide insight into the hydrogenation process. These sites are of distorted tetrahedral or distorted octahedral shape, depending on whether they are defined by four or six metallic atom vertices. The spaces contained within them generally span the entire interior of the storage substance, with incomplete (or "open") holes at the surfaces, where one or more vertices may be missing. The hydrogens are known to prefer the tetrahedral sites in some storage materials (for example, in TiH_2) and the octahedral sites in some others (for example, in NiH and PdH) [6]. The types of sites which become occupied, and the mobility of the hydrogens between the various possible sites, are determined by a delicate balance of geometric, electronic, thermodynamic, and kinetic factors [1]. We have examined the tetrahedral sites in greater detail, and introduced parameters to describe their sizes and shapes. The extension of the same type of analysis to describe octahedral sites can be carried out in a straightforward manner.

Consideration of the sizes and shapes and spatial distribution of hole sites using survey techniques, coupled with electronic structure calculations on large numbers of selected structures, is clearly seen to be a fruitful approach to the study of hydrogen storage in metal hydrides. Unfortunately, time-dependent processes such as diffusion are much more difficult to investigate by any of these techniques, but the insights obtained are likely to be valuable in approaching these problems as well.

The theoretical procedures and results are presented in Sect. 2, and the various concepts introduced and results obtained are discussed in Sect. 3. Some of our basic conclusions are summarized and future directions which the work might take are indicated in Sect. 4.

2. Theoretical procedures and results

Ab initio calculations

A series of non-empirical, all electron SCF calculations was undertaken on a few small metallic clusters, to help calibrate the Extended Hückel results on larger systems. The computations were carried out at the Unrestricted Hartree-Fock (UHF) level with the Gaussian 80 series of programs [7] running on a VAX 11/780. Some of the results of nearly 300 h of CPU time are summarized in Tables 1 and 2.

Since our initial intention was to examine several tetrahedral and octahedral clusters with and without hydrogen, we began with a small minimal basis set

Table 1. Basis set effects in *ab initio* calculations on Ti_4 and Ti_4H clusters[a]

Cluster	Basis set	Total energy (au)	$\bar{\Sigma}_H$ (eV)	$\overline{\Delta E}$ (eV)	E_H (eV)[b]	$\bar{q}_H$
Ti_4	STO-3G (atomic exp.)[c]	−3359.1995				
Ti_4H	STO-3G (atomic exp.)[c]	−3359.6650	−0.03	2.54	−18.5, −16.7	−0.38
Ti_4	STO-3G (opt. exp)[d]	−3359.2453				
Ti_4H	STO-3G (opt. exp.)[d]	−3359.7330	0.20	1.94	−17.5, −16.0	−1.03
Ti_4	Split Valence[e]	−3389.8605				
Ti_4H	Split Valence[e]	−3390.4237	−1.73	0.02	−20.1, −19.1	−0.71

[a] See Table 4 for notation; r(Ti-Ti) = 2.814 Å

[b] The energies of the α and β MO's with significant H contribution

[c] $\zeta_{3d} = 2.68$, $\zeta_{4sp} = 1.21$ for titanium [8]; $\zeta_{1s} = 1.0$ for hydrogen

[d] $\zeta_{3d} = 2.77$, $\zeta_{4sp} = 1.32$ for titanium optimized in Ti_4; hydrogen exponent optimized in Ti_4H with Ti exponents fixed at their optimum values in Ti_4, $\zeta_{1s} = 0.85$

[e] Huzinaga basis set [12] for Ti, with a (2, 1) split of the 4s, and a (3, 1) split of the 3d shells; 311G for hydrogen [13]

(STO-3G, [8]). Atom-optimized exponents were felt to be more appropriate than ones optimized for organometallic complexes. Despite the use of minimal basis sets, the cluster calculations were characterized by SCF convergence difficulties. Atomic Ti is a $3d^2 4s^2$ triplet at the UHF/STO-3G level. For tetrahedral Ti_4 (r(Ti-Ti) = 2.814 Å), the lowest energy state has a multiplicity of 9 and corresponds to an atomic configuration of $3d^{1.8} 4s^{1.3} 4p^{0.9}$. For Ti_4H (multiplicity = 10), the central hydrogen has a Mulliken population of 1.38 electrons, indicating substantial transfer of electron density from the metal to the hydrogen. Similar calculations on tetrahedral Ni_4 (r(Ni-Ni) = 2.492 Å) showed severe SCF convergence problems and yielded unrealistically high occupations of the 4p orbitals and large spin contaminations.

To test the appropriateness of the atomic exponents and to increase the flexibility of the minimal basis set calculations, we optimized the 3d and 4sp exponents in Ti_4. The optimized values ($\zeta_{3d} = 2.77$, $\zeta_{4sp} = 1.32$) are more like the atomic exponents (2.68, 1.21) than average values for organometallic complexes ($\zeta_{3d} =$ 1.90, $\zeta_{4sp} = 1.70$). This justifies, to some extent, the choice of atomic exponents and the use of the Extended Hückel parameters of Lohr and Pyykkö [9] (see below) instead of the standard values used in organometallic calculations [10]. When the exponents optimized for Ti_4 were used for Ti_4H, $\zeta_{1s} = 0.85$ was obtained for the optimum hydrogen 1s exponent. The Mulliken charge on hydrogen (2.03 electrons) is rather exaggerated because of the inadequacies of the minimal Ti basis set. Since exponent optimization had very little effect on the 4p populations in Ti_4, it is probable that optimization of the STO-3G exponents in Ni_4 will not remedy the deficiencies in the Ni_4 calculations.

It is generally recognized that at least two sets of d functions are required for the correct treatment of bonding in metal complexes [11]; however, double zeta

Table 2. Comparison of *ab initio* and Extended Hückel calculations on small metallic clusters and their hydrides[a]

			Ab initio			Extended Hückel		
Cluster	Symmetry	Bond distances (Å)	Total energy (au)	$\bar{\Sigma}_H$ (eV)	Charges	Total energy (eV)	$\bar{\Sigma}_H$ (eV)	Charges
Ti_4	T_d	TiTi = 2.814	−3389.8605		$\bar{q}_{Ti} = 0.0$	−197.27	—	$\bar{q}_{Ti} = 0.0$
Ti_4H	T_d	TiTi = 2.814	−3390.4238	−1.73	$\bar{q}_{Ti} = 0.18$	−215.23	−4.35	$\bar{q}_{Ti} = 0.02$
		TiH = 1.723			$\bar{q}_H = -0.72$			$\bar{q}_H = -0.06$
Ti_2Ni_2	C_{2v}	TiTi = 2.814	−4705.5658		$\bar{q}_{Ti} = -0.10$	−474.18	—	$\bar{q}_{Ti} = 0.15$
	(regular	TiNi = 2.814			$\bar{q}_{Ni} = 0.10$			$\bar{q}_{Ni} = -0.15$
	tetrahedron)	NiNi = 2.814						
Ti_2Ni_2H	C_{2v}	TiTi = 2.814	−4706.1338	−1.86	$\bar{q}_{Ti} = 0.26$	−492.08	−4.29	$\bar{q}_{Ti} = 0.27$
	(regular	TiNi = 2.814			$\bar{q}_{Ni} = 0.10$			$\bar{q}_{Ni} = 0.19$
	tetrahedron)	NiNi = 2.814			$\bar{q}_H = -0.71$			$\bar{q}_H = -0.16$
		TiH = 1.723						
		NiH = 1.723						
Ti_2Ni_2	C_{2v}	TiTi = 3.015	−4705.5298		$\bar{q}_{Ti} = -0.15$	−473.32	—	$\bar{q}_{Ti} = 0.19$
	(distorted	TiNi = 2.611			$\bar{q}_{Ni} = 0.15$			$\bar{q}_{Ni} = -0.19$
	tetrahedron)	NiNi = 3.015						
Ti_2Ni_2H	C_{2v}	TiTi = 3.015	−4706.0881	−1.59	$\bar{q}_{Ti} = 0.20$	−491.33	−4.40	$\bar{q}_{Ti} = 0.33$
	(distorted	TiNi = 2.611			$\bar{q}_{Ni} = 0.13$			$\bar{q}_{Ni} = -0.24$
	tetrahedron)	NiNi = 3.015			$\bar{q}_H = -0.67$			$\bar{q}_H = -0.18$
		TiH = 1.685						
		NiH = 1.685						
Ni_4	T_d	NiNi = 2.814	−6021.1995		$\bar{q}_{Ni} = 0.0$	−758.35	—	$\bar{q}_{Ni} = 0.0$
Ni_4H	T_d	NiNi = 2.814	−6021.6862	0.35	$\bar{q}_{Ni} = 0.19$	−773.26	−1.30	$\bar{q}_{Ni} = -0.05$
		NiH = 1.723			$\bar{q}_H = -0.77$			$\bar{q}_H = 0.18$
Ni_4[b]	T_d	NiNi = 2.492	−6021.0837		$\bar{q}_{Ni} = 0.0$	−757.29	—	$\bar{q}_{Ni} = 0.0$
Ni_4H	T_d	NiNi = 2.492	−6021.5958	−0.34	$\bar{q}_{Ni} = 0.20$	−772.36	−1.46	$\bar{q}_{Ni} = -0.05$
		NiH = 1.526			$\bar{q}_H = -0.81$			$\bar{q}_H = 0.21$

[a] See Table 4 for notation

[b] See also, the *ab initio* effective core potential SCF calculations of Basch H, Newton MD, Moskowitz JW (1980) J Chem Phys 73:4492 for the same geometry of Ni_4

basis set calculations are considerably more costly and severely limit the number and size of clusters that can be examined. As a compromise, we have chosen a Huzinaga (4333/43/4) basis set [12] with a (2, 1) split of the 4s and (3, 1) split of the 3d. To ensure that electron distributions ranging from H to H^- can be represented adequately, a triple zeta (311G) basis set [13] was chosen for hydrogen. SCF convergence was better than with the STO-3G basis set, but still quite slow (>100 cycles to reduce the average change in the density matrix to 10^{-5}). The approximate electronic configuration of Ti_4, $3d^{2.1}4s^{1.9}$ (multiplicity = 9), is much more realistic than with the STO-3G basis set and has relatively little contamination from higher spin states. Likewise, the binding energy of hydrogen, Σ_H, and the charge on hydrogen, q_H, are more reasonable than with the minimal basis set; therefore, the split valence basis sets were used for the remainder of the calculations.

Examination of a number of different spin states indicated that a multiplicity of 9 yielded the lowest energy for Ti_4 and Ni_4, and a multiplicity of 10 for the metal cluster hydrides. In Ni_4 and Ni_4H, the energy was lower for an electronic configuration on Ni of $3d^84s^2$ than $3d^94s^1$; however, it is clear that there are numerous states of similar energy, and that the addition of electron correlation could easily change the order of the states. To be consistent and so that structural effects on hydrogen binding would not be obscured, we chose a multiplicity of 9 for all of the *ab initio* calculations on the clusters involving four metals, and a multiplicity of 10 for the corresponding hydrides.

The results of *ab initio* calculations on several small metallic clusters and their hydrides are given in Table 2. These are compared with Extended Hückel calculations which are outlined in the next section. Three of the clusters (Ti_4, Ti_2Ni_2 and Ni_4), and their hydrides, are regular tetrahedra with the same metal-metal distance (2.814 Å). These clusters illustrate the role of composition in hydride binding. The effect of distortion can be seen in the Ti_2Ni_2 and Ti_2Ni_2H clusters in which the Ti-Ti and Ni-Ni distances have been increased by 0.201 Å relative to the regular tetrahedral clusters, and the Ti-Ni distance decreased by 0.203 Å. The effect of size can be judged by comparing the large (Ni-Ni = 2.814 Å) and small (Ni-Ni = 2.492 Å) Ni_4 clusters and their hydrides.

As might be expected at the Hartree-Fock level, Ti_4, Ti_2Ni_2 and Ni_4 are not bound relative to the free atoms. In Ti_4H, Ti_2Ni_2H and the smaller Ni_4H, the hydrogen is bound relative to the cluster plus H atom, but not relative to the cluster plus $1/2H_2$. On the other hand, the Extended Hückel results yield much more reasonable binding energies for the H atom relative to $1/2H_2$; however, the trends in binding energies are quite similar. In both the *ab initio* and the Extended Hückel calculations, the hydrogen atom is much more strongly bound in the Ti_4H and Ti_2Ni_2H clusters than in the Ni_4H clusters. The two levels of calculations also agree on the fact that decreasing the size of the Ni_4 cluster increases the binding energy for hydrogen, although this effect is smaller in the Extended Hückel calculation. The only disagreement in the trends is the effect of distorting the Ti_2Ni_2 cluster on H binding.

In each of the hydrides, the Mulliken population analysis in the *ab initio* calculations attributes too much negative charge to the hydrogen due to the diffuse functions on H. Likewise, the basis functions on Ti are more spread out and more flexible than those on Ni. Therefore, when Ti and Ni are bonded, the Mulliken population analysis makes the Ti atom too negative. Because of these problems, as well as the differences in spin states, the *ab initio* Mulliken charges cannot be compared *directly* with the Extended Hückel results. Nevertheless, one important trend can still be discerned. Both the *ab initio* and the Extended Hückel results agree that, in the Ti_2Ni_2H clusters, most of the electron density transferred to the hydrogen comes from the titanium atoms, while the Mulliken charge on nickel is almost unchanged.

Figure 1 shows the *ab initio* molecular orbital energies obtained at the unrestricted Hartree-Fock level. The lowest-lying totally symmetric *ab initio* valence orbitals of Ti_4, Ti_4H, Ni_4 and Ni_4H are displayed in Fig. 2. In Ti_4H, the molecular orbital dominated by the hydrogen 1s atomic orbital lies lower in energy than those derived from the metal 3d and 4s atomic orbitals, and thus is doubly occupied. This is reflected in the large negative charge on H. In Ni_4H, the hydrogen 1s orbital lies above the metal 3d but below the 4s, and mixes strongly with the appropriate symmetry adapted combinations of the 3d and the 4s orbitals. Strong mixing with the lowest energy (totally symmetric) combinations of the 3d orbitals is also found in SCF-Xα-SW calculations on Ni_4H [3y].

Extended Hückel calculations

Extended Hückel [5] calculations were carried out with the FORTICON8 software package [10] on an IBM 3033U computer. The largest of the cluster calculations described below took just under 11 min of CPU time.

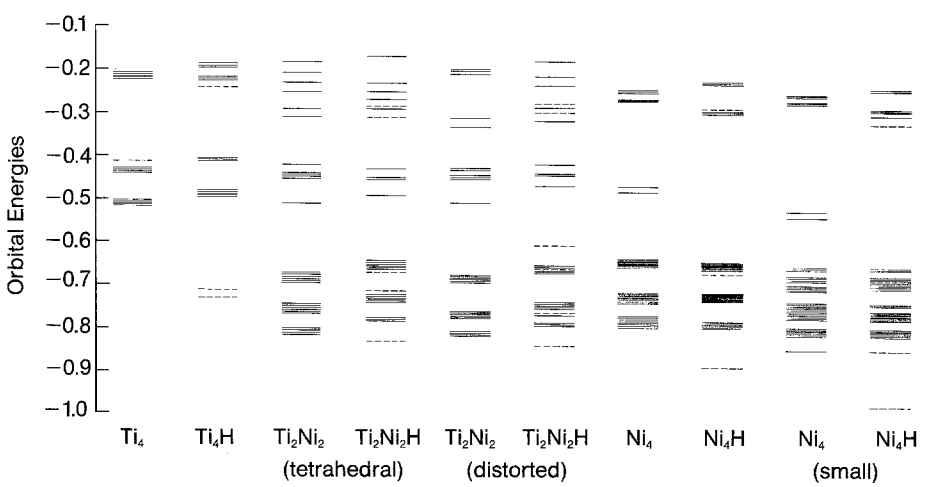

Fig. 1. One-electron energies of the occupied orbitals (alpha and beta) in au. Details of the structures are given in Table 2. Orbitals of predominantly hydrogen character are *dashed*

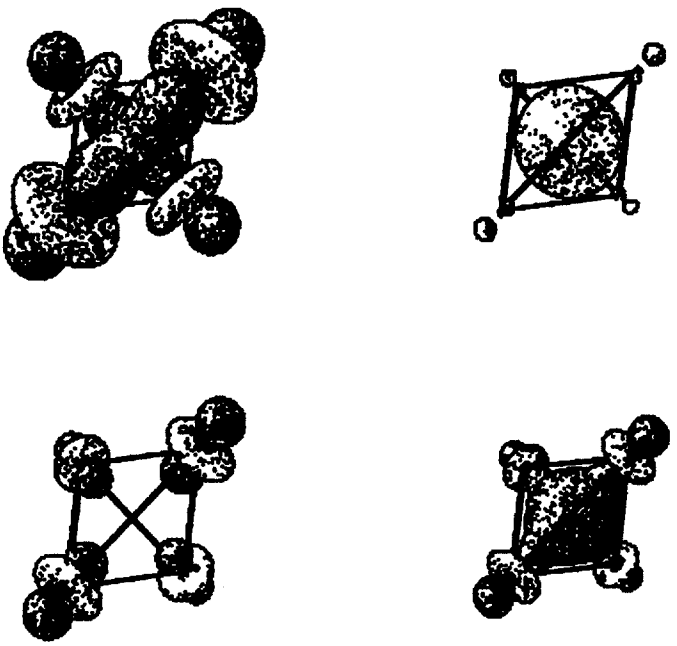

Fig. 2. Lowest-lying totally symmetric *ab initio* valence orbitals of Ti_4, Ti_4H, Ni_4 and Ni_4H

The orbital exponents and Coulomb integrals used are listed in Table 3. Since no semi-empirical parameterization designed specifically for describing the properties of metal hydride systems is available, the values for the Coulomb integrals were chosen from the non-relativistic parameterization [9] of Desclaux' atomic Dirac–Fock calculations [14]. Although there are certain drawbacks of this set of values (for example, the depth of the 3d levels of Ni is overestimated),

Table 3. Orbital exponents and coulomb integrals[a]

	s orbitals			p orbitals			d orbitals					
Atom	n	exp	coul	n	exp	coul	n	exp d_1	exp d_2	coul	c_1	c_2
H	1	1.0	−13.606	—	—	—	—	—	—	—	—	—
Ti[b]	4	1.075	−6.039	4	0.675	−3.863	3	4.55	1.4	−11.04	0.42061	0.78391
Ni[b]	4	1.825	−7.532	4	1.125	−4.284	3	5.75	2.0	−18.97	0.5683	0.6292
Cu[b]	4	1.95	−6.49	4	1.2	−3.359	3	5.95	2.1	−13.37	0.57696	0.61675
Fe[b]	4	1.575	−7.079	4	0.975	−4.183	3	5.35	1.8	−16.54	0.53659	0.66779
Ti[c]	4	1.195	−6.039	4	0.998	−3.863	3	2.353	—	−11.04	—	—
Ni[c]	4	1.473	−7.532	4	1.203	−4.284	3	3.62	—	−18.97	—	—

[a] n denotes the principal quantum number, exp the orbital exponent, and coul the coulomb integral. For the double zeta d orbitals, c_1 and c_2 denote the contraction coefficients of the two d orbitals with exponents exp d_1 and exp d_2, respectively

[b] Double zeta d orbitals

[c] Single zeta d orbitals, used in some additional calculations for comparison (see text)

its use provides a theoretically consistent way of treating these systems, without introducing any semi-empirical parameters. (See Sect. 3 for more detailed discussion of this point.)

The densities of states of these metallic clusters can only be calculated in a satisfactory manner if each set of d orbitals is treated by contracted d orbitals which are linear combinations of two *d*-type Slater functions. If only one d orbital exponent is used per atom, the bands become unrealistically narrow and sharp due to the inflexibility of such a basis set. Thus, all calculations were carried out using contracted *d* orbitals on each transition metal atom, the exponents and contraction coefficients being chosen as the values suggested by the program documentation [10, 15]. The atomic orbital exponent value of 1.0 was found to describe the 1s orbital of H much better than the value 1.3 usually used in calculations on molecules where H forms a normal chemical bond, such as most organic compounds. Here, just as the double zeta representation allows the transition metal d orbitals to interact better with one another, the exponent value of 1.0 allows the hydrogen, which acts as an alloying element with four or six near neighbors, to utilize its 1s orbital much more effectively, to expand and to form stronger links to its transition metal neighbors.

Even when an exponent value of 1.0 is used for H, the effect of its introduction is still somewhat underestimated, as will be shown below when the energetics are discussed. This is because the contracted pairs of *d* orbitals used for the metals allow stronger bonding for these atoms than the single 1s orbitals can allow for H. Since it was not practical to use a contracted 1s orbital for H, a few calculations were carried out on the Ti–Ni–H systems by representing the Ti and Ni 3d orbitals by a single exponent each (last two rows of Table 3) [9, 14]. This enabled us to assess the amount of underestimation of the energetic effect of H on these clusters, by treating all atoms at an equal level of flexibility.

Relativistic effects [16] can also be expected to produce a small effect on the densities of states. For example, Desclaux' atomic relativistic Dirac–Fock calculations [14] show that the 3*d* levels of Ni split into two sets separated by 0.277 eV, due to spin-orbit effects. These effects could be much more significant for heavier elements such as the lanthanides, actinides, and the elements on the sixth row of the periodic table. However, they can be justifiably neglected for fourth row elements such as Ti, Ni, Cu and Fe, and were therefore not considered in this work.

The sizes of the clusters to be utilized in the electronic structure calculations was considered next. This depends on the properties or processes under consideration. For example, proper treatment of the problem of hydrogen embrittlement [17] in metals might require calculations on clusters of several hundred atoms followed by finite-element calculations to deal with the macroscopic propagation of cracks [17a], or alternatively, embedded atom techniques [17b]. Another study [18], which applied the spin density functional formalism to the study of a hydrogen impurity within the context of a "jellium" cluster model, showed that a large cluster size (about 100 atoms) was needed to obtain an accurate description of some electronic properties of the impurity, although a partial cancellation of

Table 4. Energetics and average atomic charges for $Ti_{18}Ni_{18}$, $Ti_{18}Ni_{18}H_{12}$, $Ti_{24}Ni_{12}$, $Ti_{24}Ni_{12}H_{12}$, $Ti_{16}Cu_{16}$, $Ti_{24}Cu_{12}$, $Ti_{16}Fe_{16}$, $Ti_{16}Fe_{16}H_9$, and $Ti_{16}Fe_{16}H_{32}$ clusters[a,b]

Quantity \ Cluster	$Ti_{18}Ni_{18}$	$Ti_{18}Ni_{18}H_{12}$	$Ti_{24}Ni_{12}$	$Ti_{24}Ni_{12}H_{12}^{c}$	$Ti_{24}Ni_{12}H_{12}^{d}$	$Ti_{16}Cu_{16}$	$Ti_{24}Cu_{12}$	$Ti_{16}Fe_{16}$	$Ti_{16}Fe_{16}H_9$	$Ti_{16}Fe_{16}H_{32}$
E_{LUMO}	−11.139	−11.110	−11.239	−11.171	−11.192	−10.5657	−10.806	−11.508	−11.552	−11.708
E_F	−11.228	−11.160	−11.244	−11.183	−11.221	−10.5660	−10.890	−11.551	−11.579[e]	−11.761
E_G	−13.407	−13.068	−13.917	−13.161	−13.180	−12.838	−13.191	−12.879	−12.451	f
E_{HT}	—	−13.095	—	−13.789	−14.038	—	—	—	−12.519	f
E_{HB}	—	−17.893	—	−17.359	−18.172	—	—	—	−15.220	f
E_{MT}	−18.174	−18.255	−18.334	−18.419	−18.419	−12.863	−13.206	−15.236	−15.433	f
E_{MB}	−19.911	−20.305	−19.952	−20.512	−20.742	−14.400	−14.404	−18.090	−19.109	−19.521
δ_{Ti}	2.179	1.908	2.673	1.978	1.959	2.272	2.301	1.328	0.872	f
δ_H	—	4.798	—	3.570	4.134	—	—	—	2.701	f
δ_M	1.737	2.050	1.618	2.093	2.323	1.537	1.198	2.854	3.676	f
Δ_{TiH}	—	0.027	—	0.628	0.858	—	—	—	0.068	f
Δ_{HM}	—	0.362	—	1.060	0.247	—	—	—	0.213	f
Δ_{TiM}	4.767	5.187	4.417	5.258	5.239	0.025	0.015	2.357	2.982	f
Σ	−4290.486	−4506.241	−3460.434	−3673.968	−3674.941	−3107.624	−2942.275	−3061.792	−3216.440	−3616.251
$\bar{\Sigma}_H$	—	−4.374	—	−4.189	−4.270	—	—	—	−3.577	−3.721
$\overline{\Delta E}$	—	0.0005	—	0.186	0.105	—	—	—	0.797	0.653
CE	4.022	—	6.024	—	—	9.296	9.937	13.551	—	—
$\bar{q}_{Ti}$	0.166	0.286	0.1235	0.195	0.190	−1.091	−0.594	1.706	1.856	2.102
$\bar{q}_M$	−0.166	−0.179	−0.247	−0.234	−0.222	1.091	1.188	−1.706	−1.798	−1.741
$\bar{q}_H$	—	−0.161	—	−0.155	−0.157	—	—	—	−0.105	−0.180

[a] The notation is as follows:

E_{LUMO} = Energy of the lowest unoccupied molecular orbital (MO) for the cluster;
E_F = Fermi Energy, i.e., the energy of the highest occupied MO;
E_G = Lowest with predominantly Ti contributions;
E_{HT} = Highest with predominantly H contributions;
E_{HB} = Lowest with predominantly H contributions;
E_{MT} = Highest with predominantly M contributions (M = Ni, Cu or Fe);
E_{MB} = Lowest with predominantly M contributions;
$\delta_{Ti} = E_F - E_G$;
$\delta_H = E_{HT} - E_{HB}$;
$\delta_M = E_{MT} - E_{MB}$;
$\Delta_{TiH} = E_G - E_{HT}$;
$\Delta_{HM} = E_{HB} - E_{MT}$;
$\Delta_{TiM} = E_G - E_{MT}$;
Σ = Total energy, i.e., the sum of the energies of all occupied one-electron levels;
$\bar{\Sigma}_H = 1/n[\Sigma(Ti_lM_mH_n) - \Sigma(Ti_lM_m) - n\Sigma(H)]$;
$\overline{\Delta E} = 1/n[\Sigma(Ti_lM_mH_n) - \Sigma(Ti_lM_m) - 0.5n\Sigma(H_2)]$;
CE = Cohesive energy (see text for definition);
$\bar{q}_{Ti}$, $\bar{q}_M$, and $\bar{q}_H$ = The average net charge on the Ti, M, and H atoms in the cluster, obtained by a Mulliken Population Analysis.

[b] All energies are in electron volts

[c,d] These two $Ti_{24}Ni_{12}H_{12}$ clusters have the same $Ti_{24}Ni_{12}$ framework, but different H locations (see text for description)

[e] The highest occupied MO is only singly occupied in $Ti_{16}Fe_{16}H_9$, which has an odd number of electrons

[f,d] It was impossible to classify the levels for $Ti_{16}Fe_{16}H_{32}$ meaningfully into groups of Ti, H, and Fe levels

errors could be achieved by comparing the results of calculations with and without the impurity. Fortunately, for the types of properties of interest to us (such as densities of states, the positions of the energy levels, changes per hydrogen of the total energy upon hydrogenation, and Mulliken charge distributions), convergence to the bulk properties is very rapid. For example, it has recently been shown that a Be_{22} cluster can already adequately represent many aspects of the chemisorption of atomic hydrogen on the (0001) surface of beryllium, while a Be_{36} cluster is very close to the bulk limit [19]. Our own preliminary calculations on small clusters of various sizes supported this result, and showed that for the properties mentioned above the convergence with increasing lattice size was very rapid. Consequently, we carried out our calculations on clusters containing 32 or 36 transition metal atoms, whichever was more convenient for a crystal structure of a given symmetry.

The coordinates of the $Ti_{18}Ni_{18}$, $Ti_{24}Ni_{12}$, $Ti_{16}Cu_{16}$, $Ti_{24}Cu_{12}$, $Ti_{16}Fe_{16}$, and $Ti_{16}Fe_{16}H_{32}$ clusters were obtained from the appropriate experimental structural data [20]. The unit cell had to be repeated several times to obtain the $Ti_{18}Ni_{18}$, $Ti_{16}Cu_{16}$, $Ti_{24}Cu_{12}$ and $Ti_{16}Fe_{16}H_{32}$ clusters. Since the Ti_2Ni phase contains 96 atoms in its unit cell, the reverse procedure was applied and only a central portion of the unit cell was kept to obtain the $Ti_{24}Ni_{12}$ cluster. The TiFe and the TiNi phases have the same type of crystal lattice (B_2). However, since the so-called γ-phase $FeTiH_2$ required the use of only 32 transition metal atoms to get a reasonably shaped cluster, four atoms were eliminated from the 36 atom cluster for the B_2 structures to give the coordinates of $Ti_{16}Fe_{16}$.

The coordinates of $Ti_{16}Fe_{16}H_9$ were obtained from those of $Ti_{16}Fe_{16}H_{32}$ by eliminating all the hydrogens located on "open" sites at the surface, not fully surrounded by a distorted octahedron of Ti and Fe atoms. The coordinates of $Ti_{18}Ni_{18}H_{12}$ were obtained by assuming that the lattice expands to give a lattice parameter of 3.072 Å for $Ti_{18}Ni_{18}H_{12}$ (consistent with lattice parameters of 3.015 Å for the TiNi and 3.10 Å for the TiNiH phases) [21], and using a method, to be described below, to distribute twelve hydrogens among the tetrahedral holes, which have been examined in the past by other authors, in studies of the relationship of thermodynamic properties to interstitial hole sizes [22]. It has been shown experimentally [21] that the hydrogen atoms are distributed statistically in the tetrahedral holes of the TiNi lattice in the TiNiH phase. The $Ti_{24}Ni_{12}H_{12}$ clusters were obtained by using the experimentally known lattice parameter value (11.60 Å) [21] for the Ti_2NiH phase, rather than 11.3193 Å as in the Ti_2Ni phase, and using the same method to distribute twelve hydrogens between available tetrahedral sites in two different ways. The $Ti_{16}Cu_{16}H$, $Ti_{18}Ni_{18}H$ and $Ti_{24}Ni_{12}H$ clusters were obtained by taking the parent (unhydrogenated) cluster, finding the sites of various types of interest, and placing one H, in turn, into the most deeply embedded (farthest away from the surfaces) site of each type.

The energetics and average atomic charges for the $Ti_{18}Ni_{18}$, $Ti_{18}Ni_{18}H_{12}$, $Ti_{24}Ni_{12}$, $Ti_{24}Ni_{12}H_{12}$, $Ti_{16}Cu_{16}$, $Ti_{24}Cu_{12}$, $Ti_{16}Fe_{16}$, $Ti_{16}Fe_{16}H_9$, and $Ti_{16}Fe_{16}H_{32}$ clusters are listed in Table 4. In this table, E_{LUMO} refers to the energy of the lowest unoccupied molecular orbital (MO), and E_F is the Fermi energy, that is, the

energy of the highest occupied MO. E_G is the energy of the lowest-lying MO with predominantly Ti contributions, E_{HT} highest with predominantly H, E_{HB} lowest H, E_{MT} highest M (M = Ni, Cu, or Fe), and E_{MB} lowest M. The Ti, H, and M band widths are given by $\delta_{Ti} = E_F - E_G$, $\delta_H = E_{HT} - E_{HB}$, and $\delta_M = E_{MT} - E_{MB}$. The distances between various band edges are: $\Delta_{TiH} = E_G - E_{HT}$, $\Delta_{HM} = E_{HB} - E_{MT}$, and $\Delta_{TiM} = E_G - E_{MT}$. The total energy Σ is the sum of the energies of all occupied one-electron levels. $\overline{\Sigma_H}$ and $\overline{\Delta E}$ are the changes in the total energy, per hydrogen atom, in the reactions $Ti_lM_m + nH \leftrightharpoons Ti_lM_mH_n$ and $Ti_lM_m + 1/2nH_2 \leftrightharpoons Ti_lM_mH_n$, respectively. The average net charges on the Ti, M and H atoms in the cluster, obtained by a Mulliken population analysis, are given by $\bar{q}_{Ti}$, $\bar{q}_M$ and $\bar{q}_H$, respectively.

The cohesive energy (CE) is defined as follows:

$$CE(\text{bulk}) = [CE(\text{cluster} \times \bar{C}(\text{bulk})]/\bar{C}(\text{cluster})$$

where $\bar{C}$(bulk) and $\bar{C}$(cluster) refer, respectively, to the average coordination number of the atoms in the solid and in the finite-sized cluster, and the cohesive energy of the cluster is defined as:

$$CE(\text{cluster}) = \left[\sum_{j=1}^{m} (n_j E_j) - E(\text{cluster})\right] \Big/ \left(\sum_{k=1}^{m} n_k\right),$$

where E_j is the free atom energy of atom type j, and $\sum_{j=1}^{m} n_j$ is the total number of atoms in the cluster. Thus, CE(cluster) is just the stabilization energy of the cluster relative to an equal number of free atoms, per atom in the cluster. The factor $\bar{C}$(bulk)/$\bar{C}$(cluster) is included in the calculation of CE(bulk) (or CE in Table 4) to take into account the fact that the cluster contains a smaller number of the pairwise "bonding" interactions per atom than does the solid. For example, for the alloys for which we have attempted to calculate the cohesive energies, the [$\bar{C}$(cluster), $\bar{C}$(bulk)] pairs have the following values: TiNi(7.833, 14), Ti_2Ni(7.444, 13), TiCu(7.437, 14), Ti_2Cu(7.833, 14), and TiFe(7.688, 14). The atomic energies are: Ti(−44.16), Ni(−189.70), Cu(−140.19), and Fe(−132.32), while the cluster energies are given by the Σ values in Table 4. Finally, the values of the Σ(H) and $\Sigma(H_2)$ quantities used in the calculation of $\overline{\Sigma}_H$ and $\overline{\Delta E}$, are respectively −13.606 eV and −35.960 eV, where the value for H_2 has been obtained by an Extended Hückel calculation assuming the experimental value of 0.74611 Å for the bond distance [23].

Figures 3–6 depict the densities of states obtained for some of the clusters whose properties have been listed in Table 4. Since the clusters were all finite, sets of discrete molecular orbital energy levels were obtained. These were then listed in groups falling into given energy intervals, and the number of levels in each interval was plotted in the form of a histogram. The histograms were plotted in pairs to emphasize their similarities and differences. Figure 3 depicts the densities of states of $Ti_{18}Ni_{18}$ and $Ti_{18}Ni_{18}H_{12}$, Fig. 4 of $Ti_{24}Ni_{12}$ and the first of the two $Ti_{24}Ni_{12}H_{12}$ clusters, Fig. 5 of $Ti_{16}Cu_{16}$ and $Ti_{24}Cu_{12}$, and Fig. 6 of $Ti_{16}Fe_{16}$ and $Ti_{16}Fe_{16}H_{32}$.

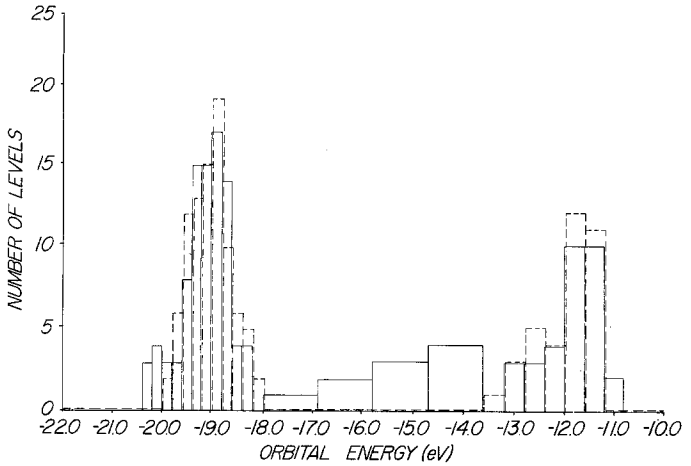

Fig. 3. Histograms depicting the occupied molecular orbital energy levels of $Ti_{18}Ni_{18}$ (*dashed lines*) and $Ti_{18}Ni_{18}H_{12}$ (*solid lines*). (Note that different histogram widths have been used at different portions of the plot, so that the number of electronic states is *not* simply proportional to the area under the histogram.)

The concept of tetrahedrality

Table 5 lists the tetrahedral hole types and their parameters, for all the binary alloys mentioned above, as well as for TiCo [20a] and the monoclinic phase of TiNi [20e]. The volume, area, and "tetrahedrality" parameters can be defined as follows: Let four points A, B, C, and D form a substructure in three dimensions, as shown in Fig. 7. Then, the total surface area of this substructure is equal to

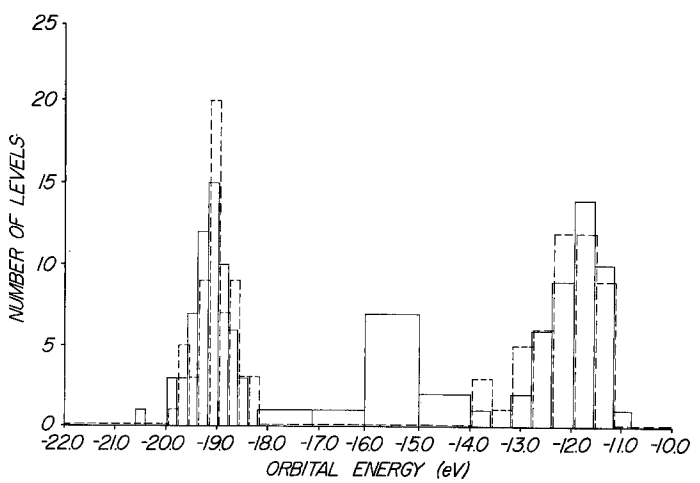

Fig. 4. Histograms depicting the occupied molecular orbital energy levels of $Ti_{24}Ni_{12}$ (*dashed lines*) and the first of the two $Ti_{24}Ni_{12}H_{12}$ clusters considered (*solid lines*). (Note that different histogram widths have been used at different portions of the plot, so that the number of electronic states is *not* simply proportional to the area under the histogram.)

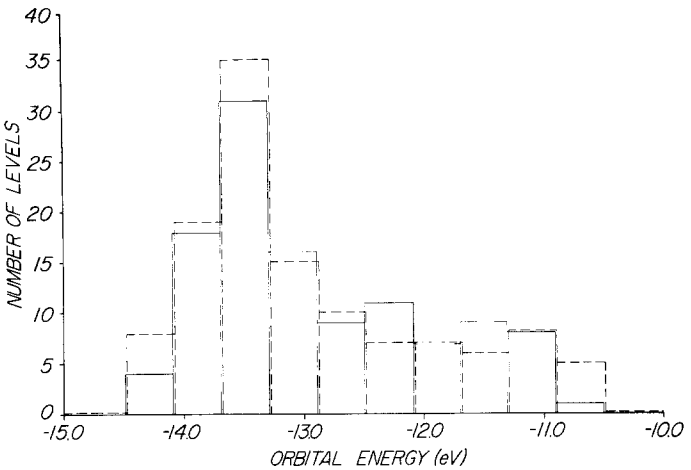

Fig. 5. Histograms depicting the occupied molecular orbital energy levels of $Ti_{16}Cu_{16}$ (*dashed lines*) and $Ti_{24}Cu_{12}$ (*solid lines*)

the sum of the areas of its four triangular faces:

$$\text{Area} = \text{Area(ABC)} + \text{Area(ABD)} + \text{Area(ACD)} + \text{Area(BCD)}.$$

(If the four points lie on the same plane, then this definition reduces to twice the area of the plane, i.e., it treats the plane like a three-dimensional solid of infinitesimal thickness.)

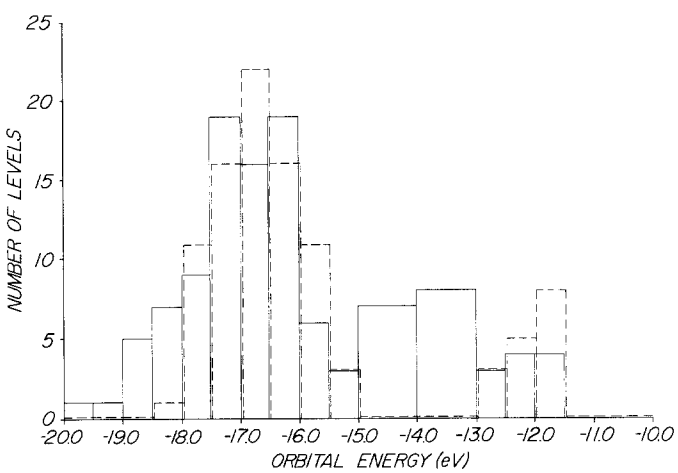

Fig. 6. Histograms depicting the occupied molecular orbital energy levels of $Ti_{16}Fe_{16}$ (*dashed lines*) and $Ti_{16}Fe_{16}H_{32}$ (*solid lines*). (Note that different histogram widths have been used at different portions of the plot, so that the number of electronic states is *not* simply proportional to the area under the histogram.)

Table 5. Tetrahedral hole types and their parameters[a]

Phase	Hole type	Volume	Area	Tetrahedrality
$TiNi(B_2)$	Ti_2Ni_2	2.2839	12.8555	0.9532
$TiCo(B_2)$	Ti_2Co_2	2.2298	12.6517	0.9532
$TiFe(B_2)$	Ti_2Fe_2	2.1964	12.5251	0.9532
TiNi	$Ti(1)_2Ni(3)Ni(4)$	2.2761	12.7231	0.9650
(monoclinic)	$Ti(2)_2Ni(3)Ni(4)$	1.5174	10.1382	0.8970
	$Ti(1)Ti(2)Ni(3)_2$	2.2761	12.5637	0.9866
	$Ti(1)Ti(2)Ni(4)_2$	3.0348	15.2585	0.9824
Ti_2Ni	$Ti(f)_3Ni$[b]	2.6779	14.0068	0.9864
	$Ti(f)_3Ni$	2.5644	13.6228	0.9843
	$Ti(f)_2Ti(c)Ni$	2.5189	13.4513	0.9858
	$Ti(f)Ti(c)Ni_2$	2.3717	12.9360	0.9841
	$Ti(c)Ni_3$	2.1489	12.0767	0.9888
	Ni_4	2.6356	13.7485	1.0
TiCu	Ti_4	2.8814	14.7504	0.9815
	Ti_3Cu	2.6413	14.2254	0.9463
	Ti_2Cu_2	2.4012	13.4182	0.9383
	$TiCu_3$	2.1610	12.2869	0.9657
	Cu_4	1.9209	12.2206	0.8574
Ti_2Cu	Ti_4	2.7730	14.2434	0.9974
	Ti_3Cu	2.6406	14.5228	0.9116
	Ti_2Cu_2	2.5082	13.4027	0.9871
	Ti_2Cu_2	2.5082	13.9309	0.9238

[a] The volume and area parameters have been obtained using the lattice parameters of the unexpanded unit cells. The number or letter in parentheses after some of the atom names, such as Ni(3) or Ti(f), refers to sites of different symmetry type for that atom

[b] This is the most common hole type for the Ti_2Ni phase

The area of each triangle can be obtained readily from vector analysis. For example, if we define $\boldsymbol{V}_1 = \boldsymbol{B} - \boldsymbol{A}$, $\boldsymbol{V}_2 = \boldsymbol{C} - \boldsymbol{A}$, and $\boldsymbol{V}_3 = \boldsymbol{D} - \boldsymbol{A}$, where $\boldsymbol{A}$, $\boldsymbol{B}$, $\boldsymbol{C}$, and $\boldsymbol{D}$ are vectors drawn from the origin of the coordinate system to the points A, B, C, and D, respectively, then:

$$\text{Area(ABC)} = 1/2|\boldsymbol{V}_1 \times \boldsymbol{V}_2|.$$

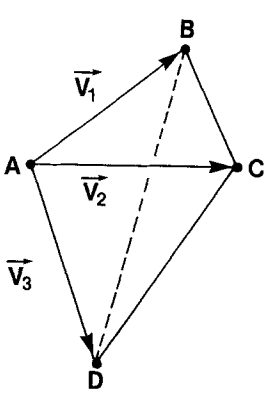

Fig. 7. A distorted tetrahedron

The volume of the distorted tetrahedron formed by the four points is given by:

$$\text{Volume} = 1/6|(\boldsymbol{V}_1 \times \boldsymbol{V}_2) \cdot \boldsymbol{V}_3|.$$

The volume is clearly zero if the four points lie on a plane. For a perfect tetrahedron, with all six side lengths equal to r, the total surface area and volume reduce to $\sqrt{3}\ r^2$ and $r^3/6\ \sqrt{2}$ respectively.

The "tetrahedrality" is defined as follows:

$$\text{Tetrahedrality} = \frac{6\sqrt{6}\,\text{Volume}}{\left[\prod_{i=1}^{6} r_i\right]^{1/6} \text{Area}}$$

where $\prod_{i=1}^{6} r_i$ is the product of the lengths of the six sides between the points A, B, C and D. The sixth root of this quantity is included in the definition. The tetrahedrality, as defined above, is clearly dimensionless and independent of overall size, dependent only on how closely the figure formed by the four points approaches a regular tetrahedron in shape, acquiring its maximum value (1.0) for a regular tetrahedron, and its minimum value (0.0) for four points falling on a plane (the most non-tetrahedral shape possible). Thus, it is a valid indicator of how closely the shape of a site approaches that of a regular tetrahedron.

Of the two $Ti_{24}Ni_{12}H_{12}$ clusters mentioned in Table 4, the first one contains eleven hydrogens in the more common type of $Ti(f)_3$ Ni sites and one in a $Ti(c)Ni_3$ site. The second $Ti_{24}Ni_{12}H_{12}$ cluster contains six hydrogens in the same type of $Ti(f)_3Ni$ sites, two in $Ti(f)_2Ti(c)Ni$ sites, three in $Ti(f)Ti(c)Ni_2$ sites, and one in a Ni_4 site.

Table 6 lists the results of some calculations on the $Ti_{18}Ni_{18}H$, $Ti_{24}Ni_{12}H$, and $Ti_{16}Cu_{16}H$ clusters whose coordinates were obtained as described above. In the $Ti_{24}Ni_{12}H$ calculations, the two Ti_3Ni sites hydrogenated are, respectively, of the $Ti(f)_2Ti(c)Ni$ and the more common $Ti(f)_3Ni$ types.

Table 7 presents a comparison of $\overline{\Delta E}$ values obtained for the $Ti_{18}Ni_{18}H_{12}$ and the two $Ti_{24}Ni_{12}H_{12}$ clusters by three different methods: (A) values listed in Table 2; (B) values extrapolated from the calculations on the clusters with only a single hydrogen; (C) values obtained using a single zeta d orbital for each metal atom; and the differences (A–B) and (A–C). See the footnotes to this table, for more details.

The surveying technique

It is well known [2, 6b] that distances of less than about 2.0 Å or 2.1 Å between non-bonded hydrogens are unfavorable due to energetic considerations related to the very strong anti-bonding H–H interactions involved (the "Switendick Criterion") [3e, f]. Assume that we are interested in finding a set of tetrahedral sites located further away from one another by at least a distance of r_c and that

Table 6. Calculations on $Ti_{18}Ni_{18}H$, $Ti_{24}Ni_{12}H$, and $Ti_{16}Cu_{16}H$ Clusters[a]

Cluster	Hydrogenated hole type	Σ	Σ_H^b	ΔE^b	E_H^c	q_H^b
$Ti_{18}Ni_{18}H$	Ti_2Ni_2	−4308.812	−4.720	−0.346	−14.828	−0.185
	$Ti_4Ni_2^d$	−4308.399	−4.306	+0.068	−14.783	−0.135
	$Ti_2Ni_4^d$	−4309.190	−5.098	−0.724	−14.948	−0.230
$Ti_{24}Ni_{12}H$	Ni_4	−3478.460	−4.420	−0.045	−14.567	−0.167
	$TiNi_3$	−3478.609	−4.569	−0.195	−14.784	−0.178
	Ti_2Ni_2	−3478.856	−4.815	−0.441	−15.115	−0.173
	Ti_3Ni^e	−3478.891	−4.851	−0.477	−15.159	−0.183
	Ti_3Ni^e	−3478.678	−4.638	−0.264	−15.601	−0.173
$Ti_{16}Cu_{16}H$	Cu_4	−3126.166	−4.936	−0.562	−16.663	−0.310
	$TiCu_3$	−3126.168	−4.938	−0.564	−16.405	−0.332
	Ti_2Cu_2	−3126.364	−5.135	−0.760	−16.516	−0.289
	Ti_3Cu	−3125.929	−4.700	−0.326	−16.472	−0.242
	Ti_4	−3125.743	−4.514	−0.140	−16.408	−0.206

[a] All energies are in electron volts

[b] These quantities do not have a bar (—) above them, since there is only one H in the clusters, and therefore no need to take an average

[c] The energy of the MO with predominantly H contribution

[d] A distorted octahedral (rather than tetrahedral) hole

[e] One of two different types of Ti_3Ni holes hydrogenated (see text)

two lattice atoms are considered to be bonded to each other if they are not further away from one another than a distance of r_B. A tetrahedral site is formed by four lattice atoms which are all within at most a distance of r_B from one another. Assume that such a group of four atoms has been found, and that the coordinates of the tetrahedral site are simply given by the average of the coordinates of these vertices of the distorted tetrahedron. Then, when a second potential tetrahedral site is found, only keep it if it is not closer than r_c to the first one. After $(n-1)$

Table 7. Comparison of ΔE values obtained by different methods

Cluster \ ΔE	Calculations			Differences	
	A[a]	B[b]	C[c]	(A-B)	(A-C)
$Ti_{18}Ni_{18}H_{12}$	0.0005	−0.346	−0.565	0.3465	0.5655
$Ti_{24}Ni_{12}H_{12}^d$	0.186	−0.258	−0.347	0.444	0.533
$Ti_{24}Ni_{12}H_{12}^d$	0.105	−0.326	−0.367	0.431	0.472

[a] Values listed in Table 4

[b] Values extrapolated by the formula $\overline{\Delta E} = 1/n \sum_{j=1}^{k} (m_j \Delta E_j)$ where n is the total number of hydrogens (here 12), the summation is over the k distinct types of holes occupied, m_j is the number of occupied holes of type j ($\sum_{j=1}^{k} m_j = n$), and ΔE_j is the ΔE value for hole type j (from values listed in Table 6)

[c] Values obtained by carrying out the calculations on the $Ti_{18}Ni_{18}$, $Ti_{18}Ni_{18}H_{12}$, $Ti_{24}Ni_{12}$, and $Ti_{24}Ni_{12}H_{12}$ clusters using a single zeta d orbital (rather than double zeta) for each metal atom

[d] One of the two different $Ti_{24}Ni_{12}H_{12}$ clusters considered (see text)

such sites, all at a distance of no less than r_c from one another, have been found, keep the next potential site only if it is not closer than r_c to any of the previously kept $(n-1)$ sites.

Clearly, the specific holes which are kept, as well as their total number and distribution according to types, will depend to some extent on the order in which the atoms are listed in the input to the computer algorithm which carries out the calculation, unless the tetrahedral holes are all of the same type, as in the B_2 phases considered. The coordinates for the hydrogens in the $Ti_{18}Ni_{18}H_{12}$ and the two $Ti_{24}Ni_{12}H_{12}$ clusters were obtained by using this algorithm and just hydrogenating 12 of the sites kept by the algorithm, in carrying out the quantum mechanical calculation. The first of the two $Ti_{24}Ni_{12}H_{12}$ hydrogen coordinate sets was obtained by listing all the Ti's first, while the second set was obtained by listing all the Ni's first. If the numbers of atoms in the clusters are allowed to increase indefinitely, and the order in which the lattice atom coordinates are fed into the computer is chosen by a completely random process (for example, by sequentially drawing cards numbered 1 through 1000 from a hat, for a cluster with 1000 atoms, and feeding in the coordinates belonging to the atom whose identification number was drawn; or by using a random number generator to reorder the atoms, which is a much more efficient randomization process), statistical limits are obtained, both for the ratio of holes kept to the total number of lattice points, and for the statistical distributions of holes of different types.

Such considerations can give fundamental insight into the amount of hydrogen uptake. For example, for the extremely simple B_2 lattices such as that in TiNi(B_2), if a cutoff value of $r_c = 2.1$ Å is chosen, the number of holes kept rapidly converges to one per Ti or Ni. That is, for a $Ti_{48}Ni_{48}$ cluster, 47 hydrogen sites are kept, consistently with the experimental fact [21] that the TiNi phase can only be hydrogenated up to a stoichiometry of TiNiH, i.e., $Ti_{48}Ni_{48}$ to a limit of $Ti_{48}Ni_{48}H_{48}$. If r_c is decreased to 2.0 Å, still only 47 sites are kept, indicating that it is impossible to force more hydrogens in without creating unfavorable interactions. For the much more complicated $Ti_{128}Ni_{64}$ cluster corresponding to two unit cells of the Ti_2Ni phase, convergence is much slower. For a calculation with $r_c = 2.0$ Å, 111 sites are kept; while for $r_c = 2.1$ Å, 90 sites are kept, when the Ti atoms in each unit cell have all been listed first in the input. The ratio $(111/90 = 1.23)$ is very close to $2.5/2.0 = 1.25$, where $Ti_2NiH_{2.5}$ and Ti_2NiH_2 are the two most heavily hydrogenated limiting stoichiometric compositions obtainable from the Ti_2Ni phase, with the last half unit of hydrogen being the most difficult to put in. Thus, it is conceivable that in Ti_2NiH_2 the hydrogens occupy sites all further away from one another by at least 2.1 Å, while the relative difficulty of making the $Ti_2NiH_{2.5}$ stoichiometry is due to the fact that many H–H distances are now on the borderline (2.0 Å–2.1 Å) of being unfavorably close to one another.

If the algorithm is carried out with $r_c < r_T$, where r_T is the closest distance allowed by the atomic arrangement in the cluster between the centers of the tetrahedral holes, then *all* the holes are kept. (Setting $r_c = 0.0$ would obviously accomplish this.) The statistical distribution of hole types is then obtained directly, regardless of how the atoms are numbered, provided that the cluster is truly representative

of the material, and large enough for it to contain a statistically significant number of each type of hole; however, in order to obtain smaller subsets of holes suitable for simultaneous occupancy by hydrogens, calculations with reasonable r_c values would still have to be carried out.

Octahedral sites

Clearly, the generalization of our algorithmic surveying procedure to include distorted octahedral sites, which could be defined and characterized by parameters in a manner similar to that used for tetrahedral sites, is fairly straightforward. For example, the "octahedrality" of a substructure formed by *six* distinct points in three dimensions, as illustrated in Fig. 8, can be defined in direct analogy with tetrahedrality:

$$\text{Octahedrality} = \frac{3\sqrt{6}\ \text{Volume}}{\left[\prod_{i=1}^{12} r_i\right]^{1/12} \text{Area}}.$$

Here, Volume is the volume of the distorted octahedron, Area is the sum of the areas of its eight triangular faces, $r_i (i = 1, 2, \ldots, 12)$ are the lengths of its twelve sides, and the twelfth root of the product $\prod_{i=1}^{12} r_i$ is included to make octahedrality dimensionless and scale-independent. The volume of the distorted octahedron illustrated in Fig. 8, is the sum of the volumes of the four distorted tetrahedra ABCF, ACDF, ADEF, and ABEF which span it.

For a perfect octahedron, with all side lengths equal to r, the total surface area and volume are $2\sqrt{3}r^2$ and $\sqrt{2}r^3/3$ respectively, giving the maximum possible octahedrality value of 1.0. The octahedrality acquires its minimum value of 0.0 for all six points falling on a plane (the most non-octahedral shape possible).

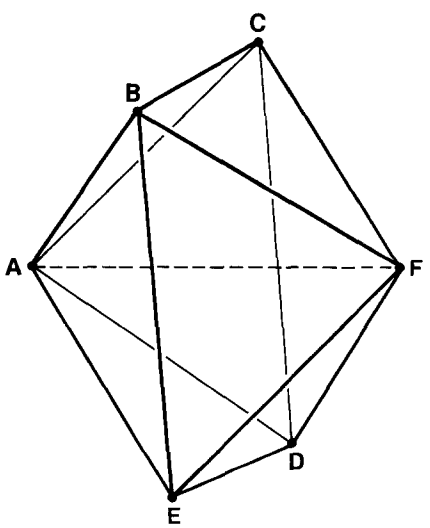

Fig. 8. A distorted octahedron

The octahedrality of the octahedral holes in B_2 phases (such as TiNi, TiCo, and TiFe [20a]) is always equal to 0.9532, just like the tetrahedrality of their tetrahedral holes.

In this connection, it should be noted that tetrahedrality and octahedrality are both special cases of the more general concept of "sphericity" [24], which quantifies how closely the shape of a polyhedron with any random number of vertices approximates a perfect sphere, which has a sphericity of 1.0.

3. Discussion

Comparison of ab initio and Extended Hückel calculations on small clusters

The results of the *ab initio* and Extended Hückel calculations on several small metallic clusters and their hydrides are compared in Table 2. For the most part, there is good qualitative agreement between the *ab initio* and Extended Hückel results. Both methods show better hydride binding when titanium is included in the cluster. Distortion of the shape of the Ti_2Ni_2 cluster has a relatively small effect on the hydride binding energy, while decreasing the size of the Ni_4 cluster causes a slight increase in the binding energy. Both *ab initio* and Extended Hückel calculations agree that the hydrogen is negatively charged, but the former method overestimates the charge considerably because of the basis set effects discussed above. In Ti_2Ni_2, *ab initio* and Extended Hückel calculations disagree in the sign of the charges; however, the two methods agree that in the formation of the hydride, the charge on the titanium changes much more than the charge on the nickel.

While the agreement between the *ab initio* and Extended Hückel calculations is not quantitative, it is clear that the most important features and trends are reproduced qualitatively. Because of the complexity of even the small clusters, *both* computational methods must be interpreted cautiously.

Extended Hückel results

The Extended Hückel method consists of a non-iterative (i.e., non-self-consistent) scheme which computes the eigenvalues and eigenvectors of the Hamiltonian by a single matrix diagonalization step. The valence electrons are then placed, in pairs, into the molecular orbitals (MO's) of lowest energy. The predominant contributions to each MO come from atomic orbitals (AO's) which have Coulomb integrals closest to the energy of that MO. For example, for the Ni atom, the ten valence electrons all go into the 3d levels, since their Coulomb integral is much lower than that of the 4s level (−18.97 eV versus −7.532 eV in the particular parameterization we used [9] as listed in Table 3). Although the effects of this electron distribution scheme and the numerical values chosen for the orbital parameters are much less pronounced in organic and organometallic systems [25] where "hybridization" is forced upon the AO's by the directional nature of the covalent bonding, they are more obvious for the binary transition metal alloy and hydride systems considered here, where the bonding is metallic and non-directional. The "charge iteration" options available in the program [10] for

crudely taking electron correlation into account, make very little improvement in the results, while increasing the computational times by about an order of magnitude, since the matrix diagonalization step now has to be repeated at each iteration. Therefore, the densities of states reported here are for the total electron density, not broken down into s and d contributions. In spite of these limitations, when the results are interpreted with full awareness of the method's strengths and weaknesses, valuable insight and semi-quantitative information can be obtained on properties such as relative energy levels, exothermicities, and charge distributions. Furthermore, by requiring only a minimal amount of computer time, the method allows large numbers of detailed calculations to be performed, as well as extensions to much larger systems than are practical for most other methods.

With these limitations in mind, the results in Table 4 and Figs. 3–6 can be analyzed as follows:

(1) The Ti–Ni and Ti–Ni–H systems are the ones for which the limitations of the computational scheme manifest themselves least. The following observations can be made about the Ti–Ni systems:
(i) The expected double peak density of states is obtained for $Ti_{18}Ni_{18}$ and $Ti_{24}Ni_{12}$, as shown in Figs. 3 and 4. The large gap between the bottom of the Ti levels and the top of the Ni levels is consistent with the large difference in the 3d Coulomb integrals used for Ti and Ni, although it is exaggerated when compared to band structure calculations [31, m]. As mentioned previously, this gap could be reduced by selecting a different set of parameters where the 3d Coulomb integrals of Ti and Ni are closer to each other, but the current values have been chosen to provide an internally consistent, non-empirical set. For example, if we choose the parameters given in [25], where the Coulomb integrals of Ti and Ni are taken to be −10.81 and −14.20 eV respectively, the Ti–Ni peak-to-peak splitting for $Ti_{18}Ni_{18}$ decreases to 2.75 eV, which is much closer to the band structure calculations [3l, m]. On the other hand, the cohesive energy of TiNi with this set of parameters is equal to 8.784 eV/atom, which is too large by approximately a factor of two (see paragraph (iv)), and the effects of the inclusion of H on the total energy and on the charge distributions are correspondingly underestimated.
(ii) The widths of the Ti and Ni portions of the density of states are reasonable. For example, metallic Ti has been shown, by ultra high vacuum photoemission measurements, to possess narrow occupied d bands of width 1.7 eV [26]. We calculate *total* Ti band widths of 2.179 and 2.673 eV for $Ti_{18}Ni_{18}$ and $Ti_{24}Ni_{12}$ respectively. These are wider than the d band width of metallic Ti since they are total band widths, with four valence electrons per Ti, rather than two. They are not *much* wider, though, since there are many fewer Ti–Ti interactions in Ti–Ni alloys than in metallic Ti. It is these strong interactions between atomic orbitals of identical energy which give the major portion of the band broadening, rather than the much weaker Ti–Ni interactions between Ti and Ni orbitals of very different energies. The widening of the Ti band in going from $Ti_{18}Ni_{18}$ to $Ti_{24}Ni_{12}$, which has more near neighbor Ti–Ti interactions per Ti atom, is consistent with

this analysis. Similarly, the band widths of the Ni levels (1.737 and 1.618 eV for $Ti_{18}Ni_{18}$ and $Ti_{24}Ni_{12}$, respectively), as well as the narrowing of the Ni band in the latter alloy, which has few near neighbor Ni–Ni interactions, are as expected.
(iii) The $Ti_{18}Ni_{18}$ and $Ti_{24}Ni_{12}$ densities of states shown in Figs. 3 and 4 are very similar, except for the differences in the band widths, and in the total electron densities in the Ti and Ni portions of the diagrams, both of these differences being a direct consequence of the different Ti/Ni ratios of the two alloys.
(iv) The E_{LUMO}, E_F, E_G, E_{MT}, and E_{MB} values are all slightly lower in $Ti_{24}Ni_{12}$ than in $Ti_{18}Ni_{18}$, indicating stronger bonding in the Ti_2Ni phase than in the TiNi phase. The cohesive energy (CE) values of $Ti_{18}Ni_{18}$ (4.022 eV/atom) and $Ti_{24}Ni_{12}$ (6.024 eV/atom) also support the idea that the Ti_2Ni phase is more strongly bonded. The cohesive energies of metallic Ti and metallic Ni are 4.85 eV/atom and 4.44 eV/atom, respectively [27]. Thus, it should be expected that $Ti_{24}Ni_{12}$ will give a slightly larger CE than $Ti_{18}Ni_{18}$; however, this difference is somewhat overestimated here, due to the positive and negative deviations of the CE values for $Ti_{24}Ni_{12}$ and $Ti_{18}Ni_{18}$, respectively, from the values that would be predicted by applying Vegard's law, i.e., taking a linear interpolation in concentration between CE values of the pure components. This is not surprising, since the cohesive energy is one of the most difficult properties to calculate using a cluster model, even when *ab initio* techniques are used [28].
(v) Consistently with the slightly greater Pauling electronegativity of Ni relative to Ti (1.91 versus 1.54) [29], the Ni atoms acquire a small average negative charge and the Ti atoms acquire a small average positive charge, in the Mulliken population analysis. Since this average charge is distributed over more Ti and fewer Ni atoms in $Ti_{24}Ni_{12}$, $|\bar{q}_{Ti}|$ is slightly lower and $|\bar{q}_{Ni}|$ is slightly higher in this cluster. However, the average $|\bar{q}|$ value over all the atoms is almost identical for the two clusters (0.166 for $Ti_{18}Ni_{18}$ and 0.165 for $Ti_{24}Ni_{12}$).

(2) The following changes take place upon inclusion of the hydrogens:
(i) A set of energy levels with predominantly hydrogen contributions appears in Figs. 3 and 4, in the gap between E_G and E_{MT}. For both $Ti_{18}Ni_{18}H_{12}$ and $Ti_{24}Ni_{12}H_{12}$, these levels are more heavily located on the Ti side than on the Ni side, consistently with the smaller separation between the Ti(3d) and H(1s) Coulomb integrals than between the H(1s) and Ni(3d) Coulomb integrals. The density of states for the second $Ti_{24}Ni_{12}H_{12}$ cluster is very similar to the first, and has not been shown. (The fact that these two $Ti_{24}Ni_{12}H_{12}$ clusters give such similar densities of states in spite of the rather different site occupancy schemes, is an interesting observation on its own right.)
(ii) The medians of the Ti and H portions of the diagrams (Figs. 3, 4) are separated by 2.929 eV for $Ti_{18}Ni_{18}H_{12}$, and 3.326 and 3.206 eV for the two $Ti_{24}Ni_{12}H_{12}$ clusters. This is consistent with the observation [26] that the peak of the H band in metallic Ti is about 5 eV below the peak of the Ti band. The δ_H values listed in Table 4 are very similar to the H band width of about 4 eV found for TiH_2 [26].
(iii) The E_{LUMO} and E_F values get pushed up slightly relative to the unhydrogenated clusters, due to some anti-bonding hydrogen admixture in what were

previously just bonding Ti levels. The E_G values go up even more. However, the lowest Ti levels have considerable H contributions, and the highest H levels have considerable Ti contributions, and this increase in E_G is partially an artifact of our artificially grouping the MO's as Ti or H levels. Thus, δ_{Ti} becomes smaller upon hydrogenation.

(iv) E_{MT} becomes a little more negative upon hydrogenation. However, the most pronounced effect at the Ni end of the diagrams is that a number of MO's, equal to the number of hydrogens in the cluster, become detached from the low end of the Ni levels, and become a tail, with a very considerable decrease in E_{MB} and increase in δ_M. This effect has been found in calculations on clusters of various sizes, as well as different numbers of hydrogens. For example, the inclusion of 1, 2, 4, 6 or 12 hydrogens in the cluster leads, respectively, to a "tail" consisting of 1, 2, 4, 6 or 12 MO levels at the low end of the Ni levels.

(v) The $\bar{\Sigma}_H$ and $\overline{\Delta E}$ values are the total energy changes in the cluster, per hydrogen atom included, if the source of hydrogen is atomic H or molecular H_2, respectively. These values are consistently underestimated by about 0.5 eV/hydrogen, for the reasons (related to basis set flexibility) discussed in Sect. 2. For example, the experimental value of $\overline{\Delta H^0}$, i.e., the enthalpy of hydrogenation defined in the same way as $\overline{\Delta E}$, is −0.436 eV/hydrogen atom obtained by breaking up H_2, for the formation of the TiNiH phase at 373°K [30]. (It should, of course, be remembered that $\overline{\Delta H}^0$ is a temperature-dependent quantity, while $\overline{\Delta E}$ is calculated at 0°K.) Our calculated value is $\overline{\Delta E} = +0.0005$ eV for the $Ti_{18}Ni_{18}H_{12}$ cluster. This subject will be discussed again later, in connection with $TiFeH_2$ phase calculations, as well as in relation to Table 7.

(vi) The $\bar{q}$ values show that H acquires an average net negative charge of about −0.16. Ni atoms become slightly more negative in $Ti_{18}Ni_{18}H_{12}$, and slightly more positive in $Ti_{24}Ni_{12}H_{12}$. In all cases, the Ti atoms lose electrons and become more positive. These results suggest the validity of a model with partially anionic hydrogens, most of the charge transfer taking place from Ti to H, to give the average partial negative charge of H.

(vii) At this point, it is instructive to compare our densities of states for the hydrides of TiNi and Ti_2Ni with the results of more accurate calculations on simpler systems such as NiH [3i] and PdH [3o]. The most significant similarities of the results are that the metallic *d*-band manifold is narrower after hydrogenation, and that there is an upward shift in the Fermi energy, and a considerable reduction of the density of states at the Fermi level, caused by this upward shift. The most significant difference is the fact that the levels with primarily H contributions lie below the metal *d* levels in the NiH and PdH calculations, while in our calculations there is both a group of hydrogen-dominated levels between the Ti and Ni levels, and a "tail" at the low energy end containing a number of levels equal to the number of hydrogen atoms in the cluster. This is again a direct consequence of the numerical value chosen, for reasons discussed above, for the 3d Coulomb integral of Ni. The choice of −14.20 eV [25] would have improved the agreement.

(3) The Ti–Cu and Ti–Fe calculations also provide very interesting results, although the deficiency of the computational scheme is somewhat more

pronounced for these calculations. For example, since the 4s orbital of Cu lies above the 3d orbital of Ti, Cu loses its 4s electron to levels of primarily Ti(3d) admixture, as can be seen from the $\bar{q}$ values. Similarly, Fe acquires a $\bar{q}$ value which is far too negative, because almost two electrons "fall" from Ti levels into the lower-lying Fe levels. We can make the following observations on these five calculations:

(i) The E_{LUMO}, E_F, E_G, E_{MT} and E_{MB} values are all lower for $Ti_{24}Cu_{12}$ than for $Ti_{16}Cu_{16}$, and the *CE* is a little larger for $Ti_{24}Cu_{12}$. These results are all consistent with the tighter binding expected for the cluster containing a larger fraction of Ti atoms (the *CE* values of metallic Ti and Cu are 4.85 and 3.49 eV/atom, respectively [27]), but the *CE* is again too large. It is also overestimated for $Ti_{16}Fe_{16}$ (*CE* (metallic Fe) = 4.28 eV/atom [27]).

(ii) δ_{Ti} has values very similar to those in the Ti-Ni phases for $Ti_{16}Cu_{16}$ and $Ti_{24}Cu_{12}$. The reason for its being very small for $Ti_{16}Fe_{16}$ is that each Ti has lost close to two electrons, so that the Ti portion of the density of states diagram is very narrow and has few electrons.

(iii) As shown in Fig. 5, because of the closeness of the 3d eigenvalues of Ti and Cu, and because of the much larger number of electrons at the Cu end, there is no obvious double peak structure. The $Ti_{16}Cu_{16}$ and $Ti_{24}Cu_{12}$ energy level structures are very similar, the main difference being in the relative numbers of levels occupied at each end.

(iv) The $Ti_{16}Fe_{16}$, $Ti_{16}Fe_{16}H_9$ (not shown) and $Ti_{16}Fe_{16}H_{32}$ calculations all give a pair of peaks for Ti and Fe, although their separation is not as great as that between the Ti and Ni peaks (see Fig. 6). The reason for the very small number of electrons at the Ti end, is again the depletion of the Ti levels. The hydrogens provide levels between the Ti and Fe bands, as well as enriching the Ti band. They also again have the effect of creating a "tail" at the low end of the energy scale and lowering E_{MB} drastically. It should be noted, however, that the partitioning of levels into Ti, H and Fe levels is far less straightforward than it was for the Ti-Ni-H alloys, since there is a much more gradual progression in relative amounts of Ti, H and Fe contributions to the MOs because the Coulomb integrals for Ti(3d) and Fe(3d) are much closer than those for Ti(3d) and Ni(3d). In fact, for the $Ti_{16}Fe_{16}H_{32}$ cluster, it was found to be very difficult to classify the levels in a meaningful manner, although the lower energy portion has predominantly Fe contributions, and the higher energy portion has predominantly Ti contributions.

(v) The $\overline{\Delta E}$ values for $Ti_{16}Fe_{16}H_9$ (0.797 eV/atom) and $Ti_{16}Fe_{16}H_{32}$ (0.653 eV/atom) are again underestimated, and should really be slightly negative. (For example, for the FeTiH system, $\overline{\Delta H}^0 = -0.145$ eV/atom [30].) See the further discussion in relation to Table 7.

(vi) It is clear from the $\bar{q}_H$ values (−0.105 for $Ti_{16}Fe_{16}H_9$ and −0.180 for $Ti_{16}Fe_{16}H_{32}$) that an anionic model with a slightly negative average partial charge on the hydrogens is favored again.

(vii) If the results presented here are compared with Gupta's work[3j,k] on β-FeTiH, which used the augmented plane wave method and a non-self-consistent potential, and provided the first calculation of the electronic structure of an intermetallic

hydride, both certain similarities and certain differences can be seen. For example, while our calculations give a set of low-lying "tail" states with strong Fe and H bonding contributions, and equal in number to the number of hydrogens in the cluster, Gupta's calculations give an even lower-lying group of states which is "detached" from the two-peak structure charcteristic of the metal states. Both our results and Gupta's results show that the lower energy portion of the metal bands has predominantly Fe contributions, and the higher energy portion has predominantly Ti contributions. On the other hand, while Gupta finds that the number of states at E_F increases substantially from FeTi to FeTiH, we find that the number of states at E_F (i.e., at the high-energy end of the histograms depicted in Fig. 6) decreases in going from the $Ti_{16}Fe_{16}$ cluster to the $Ti_{16}Fe_{16}H_{32}$ cluster. Although these comparisons are quite instructive, nevertheless, they are not conclusive since both sets of calculations used non-self-consistent computational techniques, and furthermore applied them on different hydrogenated phases of TiFe (Gupta on β-TiFeH and the present authors on γ-$TiFeH_2$).

(4) Finally, Table 4 shows that $CE(Ti_{18}Ni_{18}) < CE(Ti_{24}Ni_{12}) < CE(Ti_{16}Fe_{16})$, and $\overline{\Delta E}(Ti_{18}Ni_{18}H_{12}) < \overline{\Delta E}(Ti_{24}Ni_{12}H_{12}) < \overline{\Delta E}(Ti_{16}Fe_{16}H_n,\ n=9 \text{ or } 32)$. In other words, the more stable the original binary alloy, the weaker is the tendency to form a hydride, that is, a less exothermic $\overline{\Delta E}$ value is calculated, in agreement with Miedema's model and the rule of reversed stability [31].

Hole distribution and its relation to amount of hydrogen uptake

Table 5 lists the hole types and their parameters, as discussed in Sect. 2. It should be noted that the approach outlined in the present work is more general than the method introduced in [22], since, when used in connection with the computer algorithm also described in Sect. 2, it provides a list of *all* the types of tetrahedral holes in the system, their statistical distributions, parameters, locations, and abundances as a function of adjustable cutoff distance r_c. All that is needed is the specification of the coordinates of the atoms constituting the cluster. No analytic work is involved, the procedure is completely automatic, takes a negligible amount of computer time, and *does not depend upon or require any type of crystalline symmetry.* The sizes of the lattice atoms automatically get considered, since they are among the determining factors of the atomic coordinates in any real or model structure. If desired, considerations of hole size in terms of volume, area or radius can be more explicitly included, by eliminating all holes smaller than specified cutoff values for these parameters.

For structures analogous to those examined in [22], the volume and area parameters provide a similar ordering in terms of size as the radii of the tetrahedral holes (compare the results for $TiNi(B_2)$, $TiCo(B_2)$) and a similar correlation between the stabilities of the metal hydrides and the sizes of the tetrahedral holes, while the "tetrahedrality" provides information about the amount of deviation of the hole shapes from that of a regular tetrahedron. The approach described here can also be compared with Westlake's discussion (in an excellent recent review article) [6b] of numerous other attempts to correlate the observed

stabilities, stoichiometries and preferred hydrogen sites in hydrides of intermetallic compounds. In this review, several factors influencing stability are discussed, and it is pointed out that no single factor plays the dominant role in all systems. Westlake's paper also proposes a geometric model similar to ours in spirit that uses only a minimum hole radius (0.40 Å) and a minimum H-H distance (2.10 Å) to develop a rationale for the observed stoichiometries in hydrides of intermetallic compounds, and illustrates the model by using $LaNi_5H_{6.5}$ as an example.

It has been shown, in an analysis of the hole densities in the TiNi and Ti_2Ni phases as a function of r_c, how this type of analysis can provide valuable information about the amount of hydrogen uptake by the material, especially when the basic lattice type does not change upon hydrogenation, but merely undergoes a volume expansion. The situation is less simple for materials which undergo a change of lattice type. For example, although the B_2 phases of TiFe and TiNi have the same limiting hydrogen absorption capacity (up to stoichiometric compositions of TiFeH and TiNiH) for $r_c = 2.0$ Å, the Ti-Fe system can undergo a change of lattice type and absorb H up to a limiting stoichiometry of $TiFeH_2$. In this case, although the holes in the original B_2-type lattice were smaller in TiFe, the material becomes capable of absorbing twice as much hydrogen by undergoing a transition and acquiring a new lattice type with definite hydrogen positions [20c], rather than a statistical distribution of the hydrogens among the sites available in the original lattice.

Amorphous materials

Amorphous materials are also amenable to this type of analysis [1]. For amorphous materials, since the atoms are not located at periodic lattice points, there will be distributions of types of tetrahedral holes, with parameter values centered around several central values and having standard deviations whose sizes depend on how irregular their structure is. For example, for an amorphous analog of the crystalline Ti_2Ni phase, we could expect to find a distribution of Ti_3Ni sites, rather than the three discrete types of Ti_3Ni sites listed in Table III. We may, in addition, find a distribution of Ti_4 sites, while the crystalline Ti_2Ni phase has no Ti_4 sites at all.

Thus, under favorable experimental conditions, it is possible to force more hydrogen into an amorphous material than into an analogous crystalline material, as shown by Ovshinsky et al. [32]. Following the analysis described above, we may attribute this improved performance in part to the following:

(i) Amorphous materials generally have lower density and greater volume than analogous crystalline materials. This volume expansion makes their average hole sizes larger, and therefore the sites become more accommodating on the average. In addition, the average intersite distances increase, and thus more sites may be found to be further than a given value of r_c from one another.

(ii) Completely new types of sites will appear, for example, possibly Ti_4 sites for Ti_2Ni.

(iii) Especially in cases where groups of holes are just below the threshold of being favorable for accommodating a hydrogen (either because of intersite

distance, size, or shape considerations), many more holes may become favorable for occupancy due to the statistical distribution putting some of these sites, all of which were just below the threshold of acceptability, among sites which can accommodate hydrogen [33].
(iv) By definition, amorphous materials are metastable states, which are not absolute minima on the potential surface. When there is a crystalline analog, this analog would be the true minimum. Therefore, if the rule of reversed stability [31] holds, it would be predicted that the amorphous material, which is less stable, will have a stronger tendency to absorb hydrogen.

For the recently discussed case of TiCu [4f], a combination of these factors may be responsible for the fact that the limiting composition is TiCuH for crystalline TiCu and $TiCuH_{1.4}$ for amorphous TiCu. This is consistent with the view that the lack of a periodic lattice structure in amorphous materials should be considered as an extra degree of freedom which can be manipulated to give "tailor-made" synthetic materials with desired properties, rather than as a shortcoming [34]. It is likely that when the preparation conditions are optimized, many amorphous alloys will be found with better reversible hydrogen storage properties than the best known crystalline or microcrystalline systems. Most of these might not even have a crystalline analog [35].

Exothermicities

Another problem that had to be addressed was whether the preference of H for certain types of sites (for example the tetrahedral Ti_4 sites in crystalline TiCu) was related to the intrinsically greater stability of a hydrogen located in such a site, or to more general geometric and electronic considerations. To gain some insight into this problem, calculations were carried out on several $Ti_{18}Ni_{18}H$, $Ti_{24}Ni_{12}H$, and $Ti_{16}Cu_{16}H$ clusters, and some of the results are presented in Table 6. Note, from the ΔE column, that there is *no* correlation between the stability of a single hydrogen in a given type of hole, and the site preference of the hydrogens when a large number of them is present. Two of the most striking examples are provided by the $Ti_{18}Ni_{18}H$ and the $Ti_{16}Cu_{16}H$ calculations. For the former, $\Delta E(Ti_2Ni_4 \text{ site}) \ll \Delta E(Ti_2Ni_2)$, while the tetrahedral Ti_2Ni_2 site is known to be preferred in TiNiH. For the latter, $\Delta E(Ti_2Cu_2) < (\Delta E(TiCu_3) \leq \Delta E(Cu_4)) < \Delta E(Ti_3Cu) < \Delta E(Ti_4)$, i.e., ΔE is *least* negative for the Ti_4 site which is favored in TiCuH. Similarly, for the $Ti_{24}Ni_{12}H$ clusters, ΔE is generally less negative if more Ti atoms are at the vertices of the tetrahedron.

Although these results may appear surprising at first sight, they are not unexpected at all if we remember that the gas-phase diatomic bond strengths of Ti–H, Ni–H, and Cu–H bonds are 38, 69 and 67 kcal/mol respectively [36]. In other words, the best exothermic hydrogen absorber among these three transition metals, titanium, which can reach a stoichiometry of TiH_2, when faced with an H atom on a one-to-one basis, bonds far more weakly to H than either nickel which can only form a limiting stoichiometry of NiH in the bulk, or copper which does not even absorb hydrogen exothermically! In our clusters, when only one hydrogen is placed in a tetrahedral or octahedral hole, its interaction with its nearest

neighbors dominates, making the actual M–H bond energies an important factor. This is, however, tempered by the presence of the rest of the lattice, and in particular by the sizes and shapes of the holes involved, so that, for example, the tiny and misshaped Cu_4 hole (see the parameter values in Table 5) gives a less negative ΔE than the Ti_2Cu_2 hole, although the Cu–H bond energy is much greater than the Ti–H bond energy. However, as more hydrogens are added, hydrogen starts acting more and more like an alloying element, and H–H interactions also become increasingly important. Thus, the spatial distribution of allowed sites of different types, the H–H interactions created by these spatial distributions, and the electronic interactions which result, are of extreme importance in determining the favored types of holes. These long-range distribution effects seem to be the true reason why in general larger holes are favored, rather than their intrinsically greater stability on accommodating an individual hydrogen.

Table 6 also lists the atomic charge acquired by hydrogen (q_H), which is again negative for all 13 calculations, in accordance with a model where the hydrogens become partially anionic. Furthermore, the actual q_H and $\bar{q}_H$ values should be even more negative than those listed in Tables 4 and 6, because of the aforementioned underestimation of the effect of hydrogens in our Extended Hückel calculations. In fact, the following simple considerations suggest that the hydrogens are likely to be partially anionic on the average in *all* transition metal hydrides: for all transition metals, the *ns* ($n = 4$, 5, or 6) valence shell atomic orbital lies above the singly occupied H(1s) orbital. Thus, even for those transition metal atoms whose Pauling electronegativity [29] is at least equal to that of H (such as Pd), there will be low-lying MO's with predominantly H contributions, to which some net electron density will inevitably flow. This will result in a negative q_H in the Mulliken Population Analysis, although individual sites might be found where a hydrogen would have a slightly positive net charge. Furthermore, if a protonic model were to hold, the anti-bonding H–H interactions would not become important limiters of the amount of hydrogen uptake as rapidly as they do [3e], and at least some transition metal hydrides with much higher hydrogen storage densities and $r_c \ll 2.0$ Å would have been possible.

Table 7 presents a comparison of $\overline{\Delta E}$ values obtained by three different methods, as described in the footnotes. The (A–B) column shows that when a large number of hydrogens is present, the energy gain per hydrogen becomes less. Thus, the $Ti_{18}Ni_{18}H_{12}$ and $Ti_{24}Ni_{12}H_{12}$ calculations give $\overline{\Delta E}$ values which are less negative by 0.35 to 0.45 eV/hydrogen than those which would be obtained by filling a set of non-interacting sites, each assumed to contribute the amount given in Table 6 to the total energy. This result is consistent with the fact that as more hydrogens are added to a system, it gradually becomes more difficult and less energetically favored to add additional hydrogens, until a limiting amount is reached. This result is also consistent with the observation that in removing the hydrogens, it gradually becomes more difficult to remove any additional hydrogens, especially the last few remaining ones.

The (A–C) column shows the effect of underestimating the exothermicity of hydrogen absorption due to the fact that the basis set allows two contracted

orbitals for the description of the transition metal 3d orbital, while only one for H(1s). When a single orbital exponent is used for all orbitals, the reactions consistently become more exothermic by about 0.5 eV/hydrogen.

4. Conclusions

Consideration of the sizes and shapes and spatial distribution of hole sites using survey techniques, coupled with approximate electronic structure calculations on large numbers of selected structures, is clearly a fruitful approach to the study of hydrogen storage in metal hydrides. One obvious generalization would be to implement the same type of algorithmic surveying procedure for distorted octahedral sites which can be defined and characterized by parameters in a manner similar to that used for tetrahedral sites. Unfortunately, time-dependent processes such as diffusion are much more difficult to investigate by any of these techniques, but the insights obtained are likely to be valuable in approaching these problems as well.

Acknowledgments. We would like to thank Henry F. Schaefer III, William N. Lipscomb, Arthur Bienenstock and John P. deNeufville for stimulating discussions, and Stanford R. Ovshinsky for initiating the project, his concepts, and discussions throughout the course of this work. Additionally, we would like to thank M. Lipton and E. M. Norman for their assistance in putting together the manuscript.

References

1. Ovshinsky SR et al., to be published (also see [32])
2. For an excellent recent review (with 161 references) of the properties and applications of metal hydrides in energy conversion systems, see: Wenzl H (1982) Int Metals Rev, 27:140–168
3. a. Papaconstantopoulos DA, McCaffrey JW, Nagel DJ (1973) J Phys F: Met Phys 3:L26
   b. Papaconstantopoulos DA (1973) Phys Rev Lett 31:1050
   c. Kallne E (1974) J Phys F: Met Phys 4:167
   d. Switendick AC (1978) In: Alefeld G, Volkl J (eds) Hydrogen in metals I. Springer, Berlin p 101
   e. Switendick AC (1978) Transition metal hydrides. Advances in Chemistry Series 167:264–282
   f. Switendick AC (1979) Z Phys Chem NF 117:89
   g. Switendick AC (1980) J Less-Common Met 74:199
   h. Gupta M, Burger JP (1981) Phys Rev B 24:7099
   i. Keller J, Castro M, de Paoli AL (1982) J Appl Phys 53:8850
   j. Gupta M (1982) Phys Lett 88A:469
   k. Gupta M (1982) J Phys F: Met Phys 12:L57
   l. Boletskaya TK, Egorushkin BE, Fadin VP (1982) Phys Stat Sol B 113:307
   m. Papaconstantopoulos DA, Kamm GN, Poulopoulos PN (1982) Solid State Commun 41:93
   n. Peterman DJ, Misemer DK, Weaver JH, Peterson DT (1983) Phys Rev B 27:799
   o. Chan CT, Louie SG (1983) ibid 27:3325
   p Griessen R (1983) ibid 27:7575
   q. Ho KM, Tao HJ, Zhu XY (1984) Phys Rev Lett 53:1586
   r. Fukai Y (1984) J Less-Common Met 101:1
   s Wicke E (1984) ibid 101:17
   t. Gupta M (1984) ibid 101:35
   u. Switendick AC (1984) ibid 101:191
   v. Vaks VG, Zein NE, Orlov VG, Zinenko VI (1984) ibid 101:493
   w. Griessen R, Driessen A (1984) Phys Rev B 30:4372

x. Rao BK, Jena P (1985) Phys Rev B 31:6726
y. Messmer RP, Salahub DR, Johnson KH, Yang CY (1977) Chem Phys Lett 51:84
z. Upton TH (1984) J Am Chem Soc 106:1561
4. a. Johnson JR, Reilly JJ (1978) Inorg Chem 17:3103
b. Cotts RM In: Hydrogen in metals I, Ref. 3d, p 227
c. Flotow HE (1979) Z Phys Chem NF 116:95
d. Weaver JH, Peterson DT (1980) J Less-Common Met 74:207
e. Schlapbach L, Scherrer HR (1982) Solid State Commun 41:893
f. Bowman RC Jr, Maeland AJ, Rhim WK (1982) Phys Rev B 26:6362
g. Saw CK, Beaudry BJ, Stassis C (1983) ibid 27: 7013
h. Bohmhammel K, Wolf G, Mädge H (1984) J Less-Common Met 101:239
i. Ref. 3n also presents experimental results
5. a. Hoffmann R (1963) J Chem Phys 39:1397
b. Hoffmann R, Lipscomb WN Jr (1962) ibid 36:2179 and 3479; and ibid 37:2872; for some recent applications to solids, see:
c. Whangbo MH, Hoffmann R (1978) J Am Chem Soc 100:6093
d. Hughbanks T, Hoffmann R (1983) ibid 105:1150 and 3528
e. Hoffmann R, Hughbanks T, Kertesz M, Bird PH (1983) ibid 105:4831
6. a. See Ref. 3e for a discussion of TiH_2 and PdH, and 4g for a discussion of the deuterated system ScD_x
b. For an excellent recent review of the concepts involved in the question of site occupancy, and of numerous other methods addressing related problems, see Westlake DG (1983) J Less-Common Met 91:1
7. Binkley JS, Whiteside RA, Krishnan R, Seeger R, DeFrees DJ, Schlegel HB, Topiol S, Kahn RL, Pople JA (1980) QCPE 13:406
8. Pietro WJ, Hehre WJ (1983) J Comput Chem 4:241; instead of a 3spd shell, a 3sp and a 3d shell are used
9. Lohr LL Jr, Pyykkö P (1979) Chem Phys Lett 62:333
10. Howell J, Rossi A, Wallace D, Haraki K, Hoffmann R: QCPE Program No. 344
11. Veillard A, Demuynck J (1977) In: Schaefer III HF (ed) Modern theoretical chemistry vol 4. Plenum, New York, pp 187–222
12. Huzinaga S (1984) Gaussian basis sets for molecular calculations. Elsevier, New York
13. Krishnan R, Binkley JS, Seeger R, Pople JA (1980) J Chem Phys 72:650
14. Desclaux J-P (1973) At Data Nucl Data Tables 12:311
15. The original references are:
(a) Burns G (1964) J Chem Phys 41:1251 for the s and p orbitals; and (b) Richardson JW, Nieuwpoort WC, Powell RR, Edgell WF (1962) ibid 36:1057
16. a. Pitzer KS (1979) Acc Chem Res 12:271
b. Pyykkö P, Desclaux J-P (1979) ibid 12:276
17. a. Baskes MI, Melius CF, Wilson WD (1981) In: Bernstein IM, Thompson AW (eds) Hydrogen effects in metals. Metallurgical Society of AIME, pp 67–75
b. Daw MS, Baskes MI (1983) Phys Rev Lett 50:1285
18. Hintermann A, Manninen M (1983) Phys Rev B 27:7262
19. Bagus PS, Schaefer III HF, Bauschlicher CW Jr (1983) J Chem Phys 78:1390
20. a. Pearson WB (1967) A handbook of lattice spacings and structure of metals and alloys vol 2. Pergamon Press, Oxford, for TiNi, TiCo and TiFe
b. Mueller MH, Knott HW (1963) Trans Met Soc of AIME 227:674, for Ti_2Ni and Ti_2Cu
c. Thompson P, Reilly JJ, Reidinger R, Hastings JM, Corliss LM (1979) J Phys F: Metal Phys 9:L61 for $FeTiD_2$, assuming that the deuteriums can each be replaced by a hydrogen at the same position
d. Metals handbook (1973) Metallography, structures and phase diagrams, 8th edn vol. 8. American Society for metals, pp 237 and 239 for TiCu
e. Otsuka K, Sawamura T, Shimizu K (1971) Phys Stat Sol 5:457 for the monoclinic phase of TiNi
21. Buchner H, Gutjahr MA, Beccu KD, Saufferer H (1972) ZF Metallk 63:497
22. Lundin CE, Lynch FE, Magee CB (1977) J Less-Common Met 56:19

23. Handbook of chemistry and physics (1979) Weast RC, Astle MJ (eds) 60th edn CRC Press, p F-217
24. Bicerano J, Marynick DS, Lipscomb WN (1978) Inorg Chem 17:3443
25. For a parameterization widely used for organometallic species, see:
(a) Lauher JW, Hoffmann R (1976) J Am Chem Soc 98:1729; (b) Summerville RH, Hoffmann R (1976) ibid 98:7240. When we attempted to use this parametrization for the binary transition metal alloy and hydride systems described in this paper, we obtained unreasonable results (preliminary calculations, results not listed).
26. Eastman DE (1972) Solid State Commun 10:933
27. Kittel C (1976) Introduction to solid state physics, 5th edition. Wiley, New York, chap 3, p 74, Table I
28. For example, the STO-3G calculations reported in Ref. 19 for the Be_{36} cluster yield CE(cluster) = 23 kcal/mol per atom. This leads to $CE = 41.4$ kcal/mol per atom after weighting by the ratio $\bar{C}$(bulk)/$\bar{C}$(cluster) = $12/6_2/_3 = 1.8$. This value is still much less than the 78 kcal/mol per atom CE of the bulk metal. (Stull DR, Prophet H (1979) JANAF thermochemical tables, 2nd edn. NSRDS-NBS 37. Superintendent of Documents, Washington, D.C.)
29. Allred AL (1961) J Inorg Nucl Chem 17:215
30. Ref. 22, Table II. Note that our definition is per H atom obtained by breaking up an H_2, while their definition is per H_2 molecule. Thus, our values are half of theirs. The conversion factor from kcal/mol to eV is 1/23.061
31. a. Mal HH van, Bushow KHJ, Miedema AR (1974) J Less-Common Met 35:65
b. Miedema AR, Boom R, DenBoer FR (1975) ibid 41:283
c. Bouten PC, Miedema AR (1980) ibid 71:147
32. Ovshinsky SR, Sapru K, Dec K, Hong KC (1984) U.S. Patent No. 4,431,561 (issued on February 14)
33. A considerable amount of work has been carried out to investigate the hole structure of computer models of non-crystalline materials. For example, see Popescu MA (1980) J Non-Cryst Solids 35, 36:549 for a discussion in terms of hole radius distributions and their relationships to some of the properties of amorphous materials
34. Ovshinsky SR (1985) (a) In: Adler D, Schwartz BB, Steele MC (eds) Physical properties of amorphous materials. Institute for Amorphous Studies Series, vol 1. Plenum Press, New York, p 105; (b) J Non-Cryst Solids 75:161
35. For a comprehensive general review of the theory of the structures of non-crystalline (i.e., "amorphous") solids, written especially for chemists, see Bicerano J, Adler D: Pure Appl Chem, in press
36. Ref. 23, pp F-222 and F-223